



HAL
open science

Post-processing scheme for modeling the lithospheric magnetic field

V. Lesur, M. Rother, F. Vervelidou, M. Hamoudi, E. Thébault

► **To cite this version:**

V. Lesur, M. Rother, F. Vervelidou, M. Hamoudi, E. Thébault. Post-processing scheme for modeling the lithospheric magnetic field. *Solid Earth Discussions*, 2012, 4, pp.1345-1378. 10.5194/sed-4-1345-2012 . insu-03583014

HAL Id: insu-03583014

<https://insu.hal.science/insu-03583014>

Submitted on 22 Feb 2022

HAL is a multi-disciplinary open access archive for the deposit and dissemination of scientific research documents, whether they are published or not. The documents may come from teaching and research institutions in France or abroad, or from public or private research centers.

L'archive ouverte pluridisciplinaire **HAL**, est destinée au dépôt et à la diffusion de documents scientifiques de niveau recherche, publiés ou non, émanant des établissements d'enseignement et de recherche français ou étrangers, des laboratoires publics ou privés.



Distributed under a Creative Commons Attribution 4.0 International License

errors is necessary. Failing to do so may lead to false conclusions about the signal sources. From a practical point of view, scientists have been relatively successful in estimating a priori the noise in gravity or magnetic data sets, however correlations between errors have been most of the time ignored. This is partly because, when known, the full covariance matrix for the data errors is generally so large that it cannot be handled easily, even on modern computers (but see Langel et al., 1989; Holme and Bloxham, 1996; Rygaard-Hjalsted et al., 1997; Holme, 2000 as examples where correlated errors are accounted for in geomagnetism).

The effects of these correlation errors are obvious in airborne, marine and satellite data. Typically, in all these type of surveys, the data are collected along linear paths and, after processing, the correlation errors become apparent as offsets between adjacent tracks. They then appear in maps and models as spurious anomalies, elongated in the direction of the tracks. An example of such an effect is shown in this manuscript for magnetic models derived from satellite data. The traditional way of dealing with this noise has been to perform a “leveling” of the data. In airborne geophysics, the approach mainly consists in deriving for each track a polynomial expression that is subtracted from the data such as to minimize data differences at the cross-over points (Hamoudi et al., 2010). The method has been also adapted to satellite magnetic data. In that case a large-scale field of external origin is fitted to a data set made of only few tracks. This allows to successfully derived magnetic field models of the lithosphere to relatively high degree. A well known example is the MF series of models – e.g. Maus et al. (2008). However the method, as applied to satellite data, has its drawbacks. The effects of its application have been carefully studied in Thebault et al. (2012) and it appears that, depending on the way the method is applied, it can lead to significant distortions of the final model. However, the weakest point of this so called “along track filtering” approach is the impossibility to estimate how much the processing applied distorts the model. For this aspect, post-processing techniques are preferable.

So far post-processing techniques have been developed and applied only to models derived from satellite gravity data – e.g. Kusche (2007). To the authors knowledge such

**Lithospheric
magnetic field
post-processing**

V. Lesur et al.

Title Page

Abstract

Introduction

Conclusions

References

Tables

Figures



Back

Close

Full Screen / Esc

Printer-friendly Version

Interactive Discussion



2.1 Theory

We consider a magnetic data set made of radial component readings along a single CHAMP satellite half-orbit during night times. For simplicity we will assume that a track follows a meridian – i.e. it corresponds to a single longitude value. Models of the core field, of the lithospheric field and of the large-scale external field are then subtracted from these data. Because the description of the external field is not very accurate, the residuals obtained along that track contain relatively long wavelengths. We assume that these residuals along this single orbit are well approximated by the radial component of an external magnetic field model that does not present time dependencies. It is hereafter named as the perturbation field and writes:

$$B_{rp}(\theta, \phi, r) = - \sum_{n,k}^N \left(\frac{r}{a}\right)^{n-1} n \epsilon_n^k Y_n^k(\theta, \phi), \quad (1)$$

where ϵ_n^k are the Gauss coefficients of degree n and order k , $a = 6371.2$ km is the Earth's reference radius, $Y_n^k(\theta, \phi)$ are the Schmidt semi-normalized Spherical Harmonics (SHs). We use along this manuscript the convention that negative orders, $k < 0$, are associated with $\sin(|k|\phi)$ terms whereas null or positive orders, $k \geq 0$, are associated with $\cos(k\phi)$ terms. We will also often use the index l for the degree and m for the order.

We consider also a model of the radial component of a magnetic field of internal origin with no temporal dependencies. This model becomes below the lithospheric noise model we want to derive:

$$\tilde{B}_{ri}(\theta, \phi, r) = \sum_{l,m}^L \left(\frac{a}{r}\right)^{l+2} (l+1) \tilde{g}_l^m Y_l^m(\theta, \phi). \quad (2)$$

It is not possible to separate external field contributions from internal field contributions for data collected along a single meridian – i.e. a single half-orbit, hence we can fit

Lithospheric magnetic field post-processing

V. Lesur et al.

Title Page

Abstract

Introduction

Conclusions

References

Tables

Figures

◀

▶

◀

▶

Back

Close

Full Screen / Esc

Printer-friendly Version

Interactive Discussion



by least-squares the residuals defined in Eq. (1) with the lithospheric model given in Eq. (2). We simply need to minimize the functional:

$$\Phi_j = \sum_i w_i |\tilde{B}_{ri}(\theta_i, \phi_j, r) - B_{rp}(\theta_i, \phi_j, r)|^2, \quad (3)$$

where θ_i are sampling points along the half-orbit, ϕ_j is the longitude of the meridian that we labeled with the subscript j and w_i are weights that are defined below.

Over 10 yr, the CHAMP satellite has collected data along a large number M of half-orbits. We assume now that for each orbit the perturbation field model defined by Eq. (1) is scaled by a number η_j and that all orbits are at the same radius r . This latter point is clearly a strong approximation but there is no obvious way to avoid it. Again, these external field contributions can be interpreted as a field of internal origin. To estimate this field, the functional we have to minimize is then:

$$\Phi = \sum_{i,j} w_i |\tilde{B}_{ri}(\theta_i, \phi_j, r) - \eta_j \cdot B_{rp}(\theta_i, \phi_j, r)|^2. \quad (4)$$

Minimizing Φ for the Gauss coefficients \tilde{g}_l^m leads to a system of equations:

$$\mathbf{A}^t \mathbf{A} \tilde{\mathbf{g}} = \mathbf{A}^t \mathbf{b} \quad (5)$$

where $\tilde{\mathbf{g}} = [\tilde{g}_l^m]_{\{l,m\}}$. The matrix product $\mathbf{A}^t \mathbf{A}$ is derived from Eqs. (4) and (2) and the elements of this product associated with the degrees and orders l, l', m, m' writes:

$$\{\mathbf{A}^t \mathbf{A}\}_{l,m,l',m'} = M \left(\frac{a}{r}\right)^{l+l'+4} (l+1)(l'+1) \langle P_l^m, P_{l'}^{m'} \rangle \Pi_{mm'} \quad (6)$$

where the product $\langle P_l^m, P_{l'}^{m'} \rangle$ is defined by $\langle P_l^m, P_{l'}^{m'} \rangle = \sum_i w_i P_l^m(\cos \theta_i) P_{l'}^{m'}(\cos \theta_i)$. The variable $\Pi_{mm'}$ has been introduced to cover three cases:

$$\Pi_{mm'} = \begin{cases} \frac{1}{M} \sum_{i=1}^M \cos m \phi_i \sin |m'| \phi_i & \text{if } mm' < 0 \\ \frac{1}{M} \sum_{i=1}^M \cos m \phi_i \cos m' \phi_i & \text{if } m \geq 0, m' \geq 0 \\ \frac{1}{M} \sum_{i=1}^M \sin |m| \phi_i \sin |m'| \phi_i & \text{if } m < 0, m' < 0, \end{cases} \quad (7)$$

Lithospheric magnetic field post-processing

V. Lesur et al.

Title Page

Abstract

Introduction

Conclusions

References

Tables

Figures

◀

▶

◀

▶

Back

Close

Full Screen / Esc

Printer-friendly Version

Interactive Discussion



and is symmetric relative to its subscripts – i.e. $\Pi_{mm'} = \Pi_{m'm}$.
The elements of the right hand side vector of Eq. (5) are:

$$\{\mathbf{A}^t \mathbf{b}\}_{l,m} = -M \sum_{n,k} \left(\frac{a}{r}\right)^{l-n+3} n(l+1) \langle P_n^{|k|}, P_l^{|m|} \rangle \epsilon_n^k \chi_m^k \quad (8)$$

Depending on the sign of the orders m and k , χ_m^k takes the following values:

$$\chi_m^k = \begin{cases} \frac{1}{M} \sum_{i=1}^M \cos m\phi_i \cos k\phi_i \eta_i & \text{if } m, k \geq 0 \\ \frac{1}{M} \sum_{i=1}^M \cos m\phi_i \sin |k|\phi_i \eta_i & \text{if } mk < 0 \\ \frac{1}{M} \sum_{i=1}^M \sin |m|\phi_i \sin |k|\phi_i \eta_i & \text{if } m, k < 0, \end{cases} \quad (9)$$

and, as for $\Pi_{mm'}$, it is symmetric relative to its subscripts: $\chi_m^k = \chi_k^m$.

For very large number M of orbits uniformly distributed along longitudes, the quantity $\Pi_{mm'}$ tends to a δ -function – i.e. $\Pi_{mm'} \simeq \left(\frac{1}{2} + \frac{1}{2}\delta_{m0}\right)\delta_{mm'}$. Further, by setting the weights w_i to $w_i = \sin \theta_i$ and assuming that the sampling points are evenly spaced over the full meridian, we have $\langle P_l^{|m|}, P_{l'}^{|m|} \rangle = \frac{4-2\delta_{m0}}{2l+1} \delta_{ll'}$, and therefore, from Eq. (6), the product matrix $\mathbf{A}^t \mathbf{A}$ is diagonal. Regarding Eqs. (8) and (9), if the η_i form a set of uncorrelated random variables, the χ_m^k are also random variables with zero mean.

The Gauss coefficients for the lithospheric noise model in Eq. (2) are then:

$$\tilde{g}_l^m = - \sum_{n,k} \left(\frac{r}{a}\right)^{l+n+1} n \frac{2l+1}{2l+2} \langle P_n^{|k|}, P_l^{|m|} \rangle \epsilon_n^k \chi_m^k \quad (10)$$

and they correspond to the noise in a lithospheric field model that would be generated by un-modeled external fields in the radial component of magnetic data. Similarly, it is straightforward to find the noise in a lithospheric field model (i.e. static internal field

model) generated by a perturbation field of internal origin. This case is relevant for signals generated in the lower E-region ionosphere (e.g. at 110 km altitude) when data are acquired at satellite altitudes. Other possible sources for this type of noise are the un-modeled induced fields generated in the conductive layers of the Earth by rapid variations of the external fields. It gives:

$$\tilde{g}_l^m = \sum_{n,k}^N \left(\frac{r}{a}\right)^{l-n} (n+1) \frac{2l+1}{2l+2} \langle P_n^{|k|}, P_l^{|m|} \rangle I_n^k \chi_m^k, \quad (11)$$

where I_n^k are the Gauss coefficients for the ionospheric and/or induced field models.

In order to understand the behaviour of the lithospheric noise model, it is important to have an estimate of the probability density function of the random variable χ_m^k . Assuming the random variable η is normally distributed with variance v^η then χ_m^k appears to be also normally distributed. The set of χ_m^k are uncorrelated with the exception that $\chi_m^k = \chi_k^m$. Further the χ_m^k have a variance v^X that depends on v^η , the number of half-orbits M , the orders k and m . Possible values of the variance v^X are given in Table 1. These variances have been derived from numerical experiments involving 20 000 independent realizations of the random variables χ_m^k calculated from the same number of uniformly distributed orbits. Figure 1 presents the histograms for few values of m and k .

In the following we consider only the noise model given by Eq. (11). The general behaviour of the noise characterized by Eqs. (11) and (10) is basically the same. In particular they have the same dependence relative to the degree l . These two noise models are only relevant for the cases where the radial components of vector data are used. The way the noise propagates in a lithospheric model is different if the three components of the vector data are fitted. The corresponding equations for that case are relatively complex and given in Appendix A.

The noise model defined in Eq. (2) has $L(L+2)$ parameters – i.e. $L(L+2)$ Gauss coefficients. This number reduces to $N(N+2)$ Gauss coefficients I_n^k with

Lithospheric magnetic field post-processing

V. Lesur et al.

Title Page

Abstract

Introduction

Conclusions

References

Tables

Figures



Back

Close

Full Screen / Esc

Printer-friendly Version

Interactive Discussion



$(2N + 1)(2L + 1) - 2N^2$ random variables χ_m^k through Eq. (11). For small values of N – e.g. $N = 10$, there is a very significant reduction of number of parameters, but the Eq. (11) is non-linear.

2.2 Examples

5 In order to understand the main characteristics of the noise model defined by Eqs. (2) and (11), we present in this section the results of forward modelling calculations for a given choice of Gauss coefficients i_n^k and one realization of the set of random variables χ_m^k . The products $\langle P_n^{|k|}, P_l^{|m|} \rangle$ are calculated numerically. These products are relatively difficult to estimate accurately as the $P_l^m(x)$ functions are oscillatory. However, an adaptive Gaussian quadrature was ultimately chosen as it gave the best results.

2.2.1 Dipole perturbation field

For this first example we use a simple model for the perturbation field of internal origin made of a single spherical harmonic $n = 1, k = 1$. Specifically, we set $i_1^1 = 1$ and $i_n^k = 0$ for $\{n, k\} \neq \{1, 1\}$. This type of noise in satellite data could result from a poor modelling of the field induced by a large-scale external field in the conductive layers of the Earth. In that case Eq. (11) reduces to:

$$\tilde{g}_l^m = \left(\frac{r}{a}\right)^{l-1} 2 \frac{2l+1}{2l+2} \langle P_1^{|1|}, P_l^{|m|} \rangle i_1^1 \chi_m^1, \quad (12)$$

and the noise in the radial component of the field of internal origin is:

$$\tilde{B}_{ri}(\theta, \phi, r') = i_1^1 2 \left(\frac{a}{r'}\right)^3 \sum_{l,m} \left(\frac{r}{r'}\right)^{l-1} \frac{(l+1)(2l+1)}{(2l+2)} \langle P_1^{|1|}, P_l^{|m|} \rangle \chi_m^1 Y_l^m(\theta, \phi), \quad (13)$$

20 where r' is the modelling radius that is set to $r' = a = 6371.2$ km in this example. As the observation radius r is expected to be larger than the modelling radius, the short

Lithospheric magnetic field post-processing

V. Lesur et al.

Title Page

Abstract

Introduction

Conclusions

References

Tables

Figures

◀

▶

◀

▶

Back

Close

Full Screen / Esc

Printer-friendly Version

Interactive Discussion



wavelengths dominate the model due to the ratio $\frac{r}{r'}$ raised to the power $l - 1$ in the right hand side of Eq. (13).

In Fig. 2, the model defined by Eq. (13) is mapped for the model coefficient $\iota_1^1 = 1$ nT, an observation radius at 300 km altitude ($r = 6671.2$ km) and the random variables χ_m^1 with variances defined in Table 1 using $\nu^l = M$. The maximum SH degree involved is $L = 120$. We observe that the noise model is symmetric relative to the equator, vanishes at the poles, and is made of East-West oscillating anomalies typical of the noise in lithospheric field model derived from satellite data. We note that these characteristics are independent from the sign of the SH order k as only the random variable χ_m^k depends of this sign in Eq. (13). The obtained symmetry of the model is due to the product $\langle P_1^{|l|}, P_l^{|m|} \rangle$ that vanishes if the Legendre function $P_l^{|m|}$ is anti-symmetric – i.e. $l - |m|$ is odd. An anti-symmetric model, vanishing at the equator but not at the poles, would have been obtained if $\iota_1^0 = 1$ nT would have been chosen in place of $\iota_1^1 = 1$ nT. These symmetry/anti-symmetry characteristics are specific to models derived from the radial component alone. It can be seen in Appendix A that these characteristics are lost when a noise model is obtained from the three vector components.

The power spectrum of the model calculated at $r' = 6371.2$ km is also plotted in Fig. 2. It presents some variability due to the use of a single SH in Eq. (12). Nonetheless, the behaviour is generally along a $(\frac{r}{r'})^{2l}$ trend as it would be expected for a white noise at satellite altitude. Although the small wavelengths overshadow the larger wavelengths, the latter are also present in the noise model. It is clear that any magnetic field model derived from satellite data is contaminated by such a noise at all wavelengths unless pertinent processing steps are applied.

2.2.2 Auroral electrojet and field aligned currents

Another expected source of noise in satellite data is associated with the auroral electrojet and/or associated field-aligned currents. We do not aim at a precise description of the disturbance field but just consider the radial component of a perturbation field of

Lithospheric magnetic field post-processing

V. Lesur et al.

Title Page

Abstract

Introduction

Conclusions

References

Tables

Figures

◀

▶

◀

▶

Back

Close

Full Screen / Esc

Printer-friendly Version

Interactive Discussion



internal origin, mapped in Fig. 3 (left), and defined by:

$$B_{rp}(\theta, \phi, r) = \sum_{n,k}^N \left(\frac{a}{r}\right)^{n+2} (n+1) r_n^k Y_n^k(\theta, \phi). \quad (14)$$

We recall that in our approach this field is scaled by a random variable with zero mean for each orbit. Therefore it is more the geometry of the field that is important here than its true value. We see that the perturbation field model is centred on the geomagnetic North pole and takes relatively large values up to 60° colatitudes. The lithospheric noise model we obtain is mapped in Fig. 3 (right). This model is also fairly well localized in latitudes as it basically vanishes in the southern hemisphere. However, it seems that the noise is propagating over all longitudes. The power spectrum of the model has essentially the same characteristic than in the previous example.

The results of this example have to be analysed with some caution since real satellite orbits deviate from the exact polar direction at high latitudes. Nonetheless, we take out from these results that there is no need to describe precisely the longitudinal dependence of the rapidly varying field to obtain realistic noise model. Therefore, in Eq. (11), the range of SH order k can be restricted to small values – e.g. $k_{\max} = 2$, even if the maximum SH degree in the model remains large – e.g. $N = 30$. This will reduce even further the number of parameters needed to describe the noise model.

3 Application to magnetic models of the lithosphere

The process we applied to generate an accurate field model is in two steps. First we estimate a rough model from satellite data using a straightforward least-squares approach. Second, in the post-processing step, we co-estimate a new lithospheric field model and a model of the noise where the output model of the first step is used as data. The final results depend on the processes applied during the two steps and therefore both are described in independent subsections below.

Lithospheric magnetic field post-processing

V. Lesur et al.

Title Page

Abstract

Introduction

Conclusions

References

Tables

Figures



Back

Close

Full Screen / Esc

Printer-friendly Version

Interactive Discussion



In order to avoid confusion between the different models we use the following notations:

1. the noise model is denoted, in the same way as in the previous section, using a “~” – e.g. $\tilde{\mathbf{B}}_i$ for the magnetic field vector,
2. the noisy lithospheric model, output of the first step, is denoted using a “^” – e.g. $\hat{\mathbf{B}}_i$,
3. the lithospheric field model output of the post processing step does not have any distinctive sign – e.g. \mathbf{B}_i .

3.1 Data set, data selection, model parameterization and model estimation

Three component vector magnetic readings acquired during the ten years of the German CHAMP satellite mission are used. The data are selected for night-times and magnetically quiet days, in the same way as data are selected for the GRIMM series of core field model (Lesur et al., 2008, 2010). However, in the present case the three components of the vector data are used and data in single star camera mode are rejected. In the usual GRIMM selection scheme, at mid and low latitudes, only the X and Y SM components are selected. A core field model and a model of the large-scale external field with its internally induced counterpart are subtracted from these data, leaving mainly the contributions from the lithosphere and the noise. The core field model and external field models used are resulting from the derivation of GRIMM-3 (Lesur et al., 2011), but this is not seen as an important point in the processing: another core field model would have been possible – e.g. CHAOS-4 (Olsen et al., 2010).

Next a first lithospheric field model up to SH degree 60 is derived, but our aim here is to reject outliers. The data corresponding to residuals larger than 3 times the standard deviation are rejected. The value of the threshold, for each data type, is given in table 2. This selection process is known to potentially affect strongly the final lithospheric field model. At mid and low latitudes only few data are rejected, and those rejected

Lithospheric magnetic field post-processing

V. Lesur et al.

Title Page

Abstract

Introduction

Conclusions

References

Tables

Figures



Back

Close

Full Screen / Esc

Printer-friendly Version

Interactive Discussion



lithospheric signal dominates but the noise is clearly visible, mainly over oceans, as elongated anomalies in the north-south direction – e.g. to the south of Australia. We point out that there are strong correlations between the estimated Gauss coefficients of the model and therefore the model cannot be truncated at an arbitrary degree without introducing artefacts.

3.2 Model post-processing

The post-processing part consists in fitting a model of the magnetic field generated in the lithosphere together with the model of noise, to a 300 km altitude map of the vertical down component of the field model $\hat{B}_i(\theta, \phi, r)$ (see Fig. 4). The noise model \tilde{B}_i we used is derived in Appendix A and is parameterized by the variable χ_m^k and the Gauss coefficients of the perturbation model i_n^k . This inverse problem that consists in fitting the noise model and the lithospheric field model to \hat{B}_{Z_i} values presents some difficulties that are described first, results are given in a second subsection.

3.2.1 Inverse problem

We map the vertical down component of the magnetic field model $\hat{B}_i(\theta, \phi, r)$ at 29 161 positions on a Gauss-Legendre grid at $r = 300$ km altitude. These data values are related to the Gauss coefficients g_l^m of the field model B_i by the relation:

$$\hat{B}_{Z_i}(\theta_i, \phi_i, r) = - \sum_{l,m}^{L=120} (l+1) \left(\frac{a}{r}\right)^{l+2} g_l^m Y_l^m(\theta_i, \phi_i) + \tilde{B}_{Z_i}(\theta_i, \phi_i, r) + \epsilon_i, \quad (16)$$

where $\tilde{B}_{Z_i}(\theta_i, \phi_i, r)$ is the vertical down component of the noise model derived in Appendix A, and ϵ_i is an unknown noise. As the maximum SH degrees in \hat{B}_i and B_i are the same, it is clear that the g_l^m can be estimated such as B_i fits exactly the values of $\hat{B}_{Z_i}(\theta_i, \phi_i, r)$, with the noise model and the ϵ_i not contributing to the problem. These latter contributions become necessary only when a priori smoothness requirements

Lithospheric magnetic field post-processing

V. Lesur et al.

Title Page

Abstract

Introduction

Conclusions

References

Tables

Figures

◀

▶

◀

▶

Back

Close

Full Screen / Esc

Printer-friendly Version

Interactive Discussion



are introduced on B_j . Hence the inverse problem consists in minimizing the functional Φ defined by:

$$\Phi = \sum_i \{ \hat{B}_{Zi}(\theta_i, \phi_i, r) - B_{Zi}(\theta_i, \phi_i, r) - \tilde{B}_{Zi}(\theta_i, \phi_i, r) \}^2 + \lambda \sum_{l,m} \frac{l(l+1)^3}{2l+1} (g_l^m)^2 \quad (17)$$

The first term insures the fit to the data $\hat{B}_{Zi}(\theta_i, \phi_i, r)$ whereas the second minimizes the integral of the squared horizontal gradient of the radial component of B_j over a sphere of radius $a = 6371.2$ km. The parameter λ controls the smoothness constraint applied on B_j .

As stated above, the noise model \tilde{B}_i (Eqs. A3 and A12) is parameterized by the variable χ_m^k and the Gauss coefficients of the perturbation model i_n^k . A possibility is to set the perturbation model coefficients i_n^k , such that the model corresponds to a dipole field, and to try to estimate the χ_m^k . The inverse problem is then linear. However, for such a choice the derived lithospheric field model B_j appears to be still contaminated by noise, probably because the perturbation model has to be more complex than a simple dipole. Therefore, there is no other option than to co-estimate the χ_m^k and i_n^k values.

As these quantities enter as products in Eq. (A12), the inverse problem is non-linear and must be solved iteratively. We want to point out that finding the χ_m^k and i_n^k values in Eq. (A12) or in Eq. (11) are two different problems with their own specific null-space and difficulties. In particular, i_n^k and i_n^{-k} values cannot be estimated independently if Eq. (11) is used. With Eq. (A12) this estimation becomes possible solely because of the way the Y component data affect the noise model. However in both cases the maximum value for n can be relatively large, whereas the maximum value of k has to be small. We used in this work a maximum value of n : $N = 20$ and a maximum value for k : $K = 1$. As noted in Sect. 2.2.2 most of the complexity in longitude of the noise model is carried by the χ_m^k ; there is no need for a large longitudinal complexity of the perturbation model.

With such settings, the number of unknown describing the noise model in Eq. (A12) is reduced to $N(2K + 1) + K - K^2$ for the i_n^k (i.e. 60 values) and $(2K + 1)(2L + 1) - 2K^2$

Lithospheric magnetic field post-processing

V. Lesur et al.

Title Page

Abstract

Introduction

Conclusions

References

Tables

Figures

◀

▶

◀

▶

Back

Close

Full Screen / Esc

Printer-friendly Version

Interactive Discussion



for the χ_m^k (i.e. 721 values for $L = 120$). These numbers have to be compared with the number of unknown in the lithospheric field model $L(L + 2) = 14640$.

The iterative inversion process we followed to reach the solution presented in the next subsection is described in three steps:

step-1 Find the g_l^m in Eq. (16) minimizing Φ (Eq. (17)) imposing $\chi_m^k = 0$ for all possible m and k values.

step-2 Keeping the g_l^m unchanged, and starting with $i_n^k = 1$ for all possible n and k values, find iteratively the i_n^k and χ_m^k that minimize Φ in Eq. (17).

step-3 Iteratively find the g_l^m , i_n^k and χ_m^k that minimize Φ in Eq. (17), starting from the output of the step 2.

3.2.2 Results

The results were obtained by iteratively minimizing the functional defined in Eq. (17) following the process described above, with the parameter λ set to $\lambda = 4.0 \times 10^{-5}$ such that the resulting field model has an acceptable power spectrum. The level of noise is larger at high latitudes in the $\hat{B}_{Zl}(\theta_i, \phi_i, r)$, we therefore weight the data by $\frac{1}{6}$ for magnetic latitudes higher than 50° .

The output of the step-1 of the iterative process is a smoothed model obtained without co-estimation of the noise model. The map of this model vertical down component at radius 6371.2 km is shown in Fig. 5. The perturbation due to the along track noise in the satellite data are strong, particularly over Antarctica, and in the Indian, Atlantic and eastern Pacific oceans. This map is given here as reference for comparison with our final model obtained by co-estimation with the noise model.

The residuals to the fit to the data after the last step of the fitting process are mapped in Fig. 6, left. The largest anomalies, as the Bangui anomaly in central Africa or the Kursk anomaly in western Russia, are clearly identifiable on this residual map, although

Lithospheric magnetic field post-processing

V. Lesur et al.

Title Page

Abstract

Introduction

Conclusions

References

Tables

Figures



Back

Close

Full Screen / Esc

Printer-friendly Version

Interactive Discussion



they are not associated with too large residuals. There are very large clusters of residuals at high latitudes, and some of these residuals obviously correspond to lithospheric magnetic anomalies – e.g. North America, Southern tip of Greenland, Northern Europe. This is an incentive to work with localized system of representation and to define local constraints. Here we want to keep the processing as simple as possible and did not follow such approaches. It should be noted, however, that the amplitude of the residuals are clearly smaller than 1 nT and that there is only few traces of the “along track” noise in these residuals. The effect of the smoothing on the model remains acceptable.

Figure 6 right, shows the power spectra of the field model B_j and of the noise model \tilde{B}_j . Also plotted is the spectrum from MF7. The damping parameter λ in Eq. (17) has been adjusted to $\lambda = 4.0 \times 10^{-5}$ such that the power spectrum does not present excessively high values at high degrees. Overall, the derived map has the same level of energy than MF7 up to degree 100. Above that degree the spectra is clearly decreasing. Our opinion is that we are reaching at these SH degrees the maximum “global” resolution of the CHAMP data selected and processed following the technique described above. Improvements are probably still possible locally, particularly above the largest anomalies seen as Bangui and Kursk anomalies.

Figure 7 maps, on the left, the noise model \tilde{B}_j , and, on the right the perturbation model defined in Eq. (A1). The noise model presents the expected East-West high frequency oscillations. The map cannot be directly compared with Fig. 5 because the patterns of the oscillations in Fig. 7 correspond to the noise present in \tilde{B}_j : the Fig. 5 is only a smoothed version of it. The perturbation model (Fig. 7, right) is dominated by a dipole term consistent with un-modelled contributions generated in 1-D conductive layers of the Earth by a large-scale, rapidly varying external field. Although this large-scale field is dominant, higher spherical harmonic contributions exist in the perturbation model and are determinant for the success of the post-processing.

Our final result is a map of the vertical down component of the lithospheric field calculated at the Earth’s surface (see Fig. 8). The map includes all SH degrees of the lithospheric field model. The model is displayed with two different central meridians for

Lithospheric magnetic field post-processing

V. Lesur et al.

Title Page

Abstract

Introduction

Conclusions

References

Tables

Figures



Back

Close

Full Screen / Esc

Printer-friendly Version

Interactive Discussion



Lithospheric magnetic field post-processing

V. Lesur et al.

Title Page

Abstract

Introduction

Conclusions

References

Tables

Figures

◀

▶

◀

▶

Back

Close

Full Screen / Esc

Printer-friendly Version

Interactive Discussion



a better view of the anomaly patterns. The anomaly patterns are not as clearly defined as in MF7, but in numerous areas – e.g. the northern pacific, the map resulting from our processing is remarkably detailed. However, in the present case, the only difference with regards to a straightfoward least-squares approach is the co-estimation of the noise model. In particular, there are no pre-processing steps such as data leveling (or micro-levelling) with mostly unknown consequences on the final map, and the only data used are the CHAMP satellite data. We have made numerous experiments, and it appears that the determinant step for the final quality of the map is the data selection used to build the model \hat{B}_j . Out of all these tries, the maps presenting the lowest level of noise are systematically the outputs of the step-2 of our processing. We decided not to show these results here because they are not consistent with the noise model presented in Appendix A that assumes a model derived through a non-regularized scheme. It is however an approach worth studying: There are no major difficulties in estimating what the noise model should be for a lithospheric model built using a regularized least-squares process.

4 Conclusions

We have calculated the gauss coefficients describing the noise leaking in lithospheric magnetic field model when derived from satellite data. The noise models were derived to cover two cases: first when exclusively the radial components of the satellite data are used and second when all three components are used. The first case would be primarily applicable to gravity data, whereas the second, as we used it here, is better suited for magnetic data. We made several strong hypotheses to obtain these results. Particularly, we consider that the orbits are exactly polar, that they are at constant radius and that the sampling rate along an orbit is “ideal” – i.e. the relation $\langle P_l^{l,m}, P_l^{l,m} \rangle \propto \delta_{ll'}$ is verified. We also make the assumption that the lithospheric field model is derived through a simple un-regularized least-squares process. We insist here on the fact that

the noise models do not represent the expected noise in the satellite data but the noise in the derived lithospheric models.

It is interesting to notice that the amplitude of the noise generated depends on the variance of the random variable χ_m^k , that itself depends on the variance of the external field scaling factor η and the number of orbits M (see Table 1). Therefore the usual choice of rejecting a significant part of the data because of its level of noise is questionable. For example when dealing with magnetic data, rejecting a full year of satellite data because of the high level of magnetic activity is unlikely to reduce the noise level in the model since the ratio $\frac{\sqrt{\eta}}{M}$ generally does not get smaller. We cannot comment however on a data rejection criteria based on the satellite altitude.

Another remarkable property of the noise models is their weak dependence with regard to the source of the noise. We used here perturbation models either from internal or external origin, but both lead to similar noise models. The same developments could be done for a noise described by spherical harmonics without reference to any specific source. For the case where only radial component data are used (Eqs. 10 and 11), such an hypothesis would not make any difference.

In the application to real data, the noise models were used in a post-processing scheme. The reason for this choice is that we did not know what kind of perturbation model $B_p(\theta, \phi, r)$ should be used. We have seen that for deriving a lithospheric field model, a dipole perturbation field is not leading to the best results. In an ideal case where the perturbation model is known, the best approach to the problem would be to build a covariance matrix C_n for the noise from the variances given in Table 1 and the Eq. (A12). Such a covariance matrix can then be used as a regularization matrix in the least-squares fit of the lithospheric field model to the satellite data. However, even if the information provided by the estimated variances has not been used in our post-processing scheme, the resulting lithospheric field model is nonetheless much improved compared to what can be obtained through a simple smoothing (see the differences between Figs. 8 and 5).

Lithospheric magnetic field post-processing

V. Lesur et al.

Title Page

Abstract

Introduction

Conclusions

References

Tables

Figures



Back

Close

Full Screen / Esc

Printer-friendly Version

Interactive Discussion



It is scaled at each orbit by a factor η and is fitted by least-squares with a field of internal origin constant in time. Therefore we minimize the functional:

$$\Phi = \sum_{i,j} w_i |\tilde{\mathbf{B}}_i(\theta_i, \phi_j, r) - \eta_j \cdot \mathbf{B}_p(\theta_i, \phi_j, r)|^2, \quad (\text{A2})$$

where the noise model $\tilde{\mathbf{B}}_i$ is defined by:

$$\tilde{\mathbf{B}}_i(\theta, \phi, r) = -\nabla \left[a \sum_{l,m}^{L=120} \left(\frac{a}{r}\right)^{l+1} \tilde{g}_l^m Y_l^m(\theta, \phi) \right]. \quad (\text{A3})$$

This leads to a linear system equivalent to Eq. (5), where the left hand side writes:

$$\{\mathbf{A}^t \mathbf{A}\}_{l,m,l',m'} = \left(\frac{a}{r}\right)^{l+l'+4} (l+1)(l'+1) \sum_{i,j} w_i Y_l^m(\theta_i, \phi_j, r) Y_{l'}^{m'}(\theta_i, \phi_j, r) \\ + \left(\frac{a}{r}\right)^{l+l'+4} \sum_{i,j} w_i \nabla_h Y_l^m(\theta_i, \phi_j, r) \cdot \nabla_h Y_{l'}^{m'}(\theta_i, \phi_j, r). \quad (\text{A4})$$

The operator ∇_h is the horizontal gradient on a sphere of unit radius. The first term in the right hand side does not present difficulties. For the second we use the identity:

$$Y_l^m Y_{l'}^{m'} = \sum_{L=|l-l'|}^{l+l'} \sum_M C_{l,l',m,m'}^{L,M} Y_L^M. \quad (\text{A5})$$

Applying twice the gradient operator gives:

$$\nabla_h Y_l^m \cdot \nabla_h Y_{l'}^{m'} = \frac{l(l+1) + l'(l'+1)}{2} Y_l^m Y_{l'}^{m'} - \frac{1}{2} \sum_{L=|l-l'|}^{l+l'} \sum_M C_{l,l',m,m'}^{L,M} L(L+1) Y_L^M. \quad (\text{A6})$$

The Eq. (A4) becomes:

$$\{\mathbf{A}^t \mathbf{A}\}_{l,m,l',m'} = \left(\frac{a}{r}\right)^{l+l'+4} \frac{(l+l'+1)(l+l'+2)}{2} \sum_{i,j} w_i Y_l^m(\theta_i, \phi_j, r) Y_{l'}^{m'}(\theta_i, \phi_j, r) \\ - \left(\frac{a}{r}\right)^{l+l'+4} \sum_{L=|l-l'|}^{l+l'} \sum_M C_{l,l',m,m'}^{L,M} \frac{L(L+1)}{2} \sum_{i,j} w_i Y_L^M(\theta_i, \phi_j, r). \quad (\text{A7})$$

Lithospheric magnetic field post-processing

V. Lesur et al.

Title Page

Abstract

Introduction

Conclusions

References

Tables

Figures

◀

▶

◀

▶

Back

Close

Full Screen / Esc

Printer-friendly Version

Interactive Discussion



Defining $\Pi_{mm'}$ as in Eq. (7) gives in the limit of a large number M of orbits

$$\Pi_{mm'} \simeq \left(\frac{1}{2} + \frac{1}{2}\delta_{m0}\right)\delta_{mm'}.$$

Further, the weights w_i are chosen such that $\sum_i w_i P_l^m(\cos\theta_i) P_{l'}^{m'}(\cos\theta_i) = \frac{4-2\delta_{m0}}{2l+1}\delta_{ll'}$, which reduces for $l' = m' = 0$ to $\sum_i w_i P_l^m(\cos\theta_i) = 2\delta_{m0}\delta_{l0}$.

5 As a consequence, for the second term in the right hand side of Eq. (A7) only the term $L = 0$ remains. It therefore vanishes because of the factor $L(L+1)$ and we obtain:

$$\{\mathbf{A}^t \mathbf{A}\}_{l,m,l',m'} = 2M \left(\frac{a}{r}\right)^{2l+4} (l+1) \delta_{ll'} \delta_{mm'}. \quad (\text{A8})$$

The matrix $\mathbf{A}^t \mathbf{A}$ is therefore diagonal: The discret summations in Eq. (A4) are equivalent to continuous integrations.

10 The product $\{\mathbf{A}^t \mathbf{b}\}_{l,m}$ in the right hand side of Eq. (5) now writes:

$$\begin{aligned} \{\mathbf{A}^t \mathbf{b}\}_{l,m} = M \sum_{n,k}^N \left(\frac{a}{r}\right)^{l+n+4} \{ & (l+1)(n+1) \sum_{i,j} \eta_j w_i Y_l^m(\theta_i, \phi_j, r) Y_n^k(\theta_i, \phi_j, r) \\ & + \sum_{i,j} \eta_j w_i \nabla_h Y_l^m(\theta_i, \phi_j, r) \cdot \nabla_h Y_n^k(\theta_i, \phi_j, r) \}. \end{aligned} \quad (\text{A9})$$

We further introduce the variable χ_m^k defined by:

$$\chi_m^k = \begin{cases} \chi_{-m}^{-k} & \text{if } mk > 0 \\ -\chi_{-m}^{-k} & \text{if } mk < 0 \\ 0 & \text{if } mk = 0, \end{cases} \quad (\text{A10})$$

where the expression of χ_m^k is given in Eq. (9). The Eq. (A9) becomes:

$$\begin{aligned} \{\mathbf{A}^t \mathbf{b}\}_{l,m} = M \sum_{n,k}^N I_n^k \left(\frac{a}{r}\right)^{l+n+4} \{ & (l+1)(n+1) \langle P_n^{|k|}, P_l^{|m|} \rangle \chi_m^k \\ & + \langle \partial_\theta P_n^{|k|}, \partial_\theta P_l^{|m|} \rangle \chi_m^k + \left\langle \frac{|k|P_n^{|k|}}{\sin\theta}, \frac{|m|P_l^{|m|}}{\sin\theta} \right\rangle \dot{\chi}_m^k \}, \end{aligned} \quad (\text{A11})$$

leading when combined with Eq. (A7) to:

$$\begin{aligned} \tilde{g}_l^m = \sum_{n,k}^N I_n^k \left(\frac{a}{r}\right)^{n-l} \{ & \frac{n+1}{2} \langle P_n^{|k|}, P_l^{|m|} \rangle \chi_m^k \\ & + \frac{1}{2l+2} \langle \partial_\theta P_n^{|k|}, \partial_\theta P_l^{|m|} \rangle \chi_m^k + \frac{1}{2l+2} \left\langle \frac{|k|P_n^{|k|}}{\sin\theta}, \frac{|m|P_l^{|m|}}{\sin\theta} \right\rangle \dot{\chi}_m^k \}. \end{aligned} \quad (\text{A12})$$

The $L(L + 2)$ gauss coefficients \tilde{g}_l^m of the noise model can be represented by only $N(N+2)$ coefficients l_n^k of the perturbation model and $(2N+1)(2L+1)-2N^2$ independent random variables χ_m^k where all symmetry properties have been accounted for.

Acknowledgements. We would like to acknowledge the work of CHAMP satellite data processing team. M. R. was supported through the DFG grant: LE 2477/3-1 in the framework of the SPP-1488 “Planetary magnetism”. IGP contribution number: 3340.

References

- Hamoudi, M., Quesnel, Y., Dymont, J., and Lesur, V.: Aeromagnetic and Marine Measurements, in: *Geomagnetic Observations and Models*, edited by: Manda, M. and Korte, M., vol. 5, IAGA book series, chap. 4, 57–105, Springer, doi:10.1007/978-90-481-9858-0, 2010. 1347
- Holme, R.: Modelling of attitude error in vector magnetic data: application to Ørsted data, *Earth Planets Space*, 52, 1187–1197, 2000. 1347
- Holme, R. and Bloxham, J.: The treatment of attitude errors in satellite geomagnetic data, *Phys. Earth Planet. In.*, 98, 221–233, 1996. 1347
- Kusche, J.: Approximate decorrelation and non-isotropic smoothing of time-variable GRACE-type gravity field models, *J. Geodesy*, 81, 733–749, doi:10.1007/s00190-007-0143-3, 2007. 1347
- Langel, R. A., Estes, R. H., and Sabaka, T. J.: Uncertainty estimates in geomagnetic field modelling, *J. Geophys. Res.*, 94, 12281–12299, 1989. 1347
- Lesur, V., Wardinski, I., Rother, M., and Manda, M.: GRIMM – The GFZ Reference Internal Magnetic Model based on vector satellite and observatory data, *Geophys. J. Int.*, 173, 382–394, doi:10.1111/j.1365-246X.2008.03724.x, 2008. 1356
- Lesur, V., Wardinski, I., Hamoudi, M., and Rother, M.: The second generation of the GFZ Reference Internal Magnetic field Model: GRIMM-2, *Earth Planets Space*, 62, 765–773, doi:10.5047/eps.2010.07.007, 2010. 1356
- Lesur, V., Wardinski, I., Hamoudi, M., Rother, M., and Kunagu, P.: Third version of the GFZ Reference Internal Magnetic Model: GRIMM-3, in: *IUGG2011, MR207*, Melbourne, Australia, 2011. 1356

Lithospheric magnetic field post-processing

V. Lesur et al.

Title Page

Abstract

Introduction

Conclusions

References

Tables

Figures



Back

Close

Full Screen / Esc

Printer-friendly Version

Interactive Discussion



Lithospheric magnetic field post-processing

V. Lesur et al.

Title Page

Abstract

Introduction

Conclusions

References

Tables

Figures

◀

▶

◀

▶

Back

Close

Full Screen / Esc

Printer-friendly Version

Interactive Discussion



Lowes, F. J. and Olsen, N.: A more realistic estimate of the variances and systematic errors in spherical harmonic geomagnetic field models, *Geophys. J. Int.*, 157, 1027–1044, 2004. 1348

Maus, S., Yin, F., Lühr, H., Manoj, C., Rother, M., Rauberg, J., Michaelis, I., Stolle, C., and Müller, R. D.: Resolution of direction of oceanic magnetic lineations by the sixth-generation lithospheric magnetic field model from CHAMP satellite magnetic measurements, *Geochem. Geophys. Geosy.*, 9, Q07021, doi:10.1029/2008GC001949, 2008. 1347, 1348

Olsen, N., Lühr, H., T. Sabaka, T., Michaelis, I., Rauberg, J., and Tøffner-Clausen, L.: CHAOS-4 – A high-resolution geomagnetic field model derived from low-altitude CHAMP data, in: AGU Fall Meeting, Poster GP21A-0992, San Francisco, 2010. 1348, 1356

Reigber, C., Lühr, H., Schwintzer, P., and Wickert, J., eds.: *Earth Observation with CHAMP Results from three years in orbit*, Springer-Verlag, 2005. 1348

Rygaard-Hjalsted, C., Constable, C. G., and Parker, R. L.: The influence of correlated crustal signals in modelling the main geomagnetic field, *Geophys. J. Int.*, 130, 717–726, 1997. 1347

Thebault, E., Vervelidou, F., Lesur, V., and Hamoudi, M.: The shortcomings of along-track satellite analysis in planetary magnetism, *Geophys. J. Int.*, 188, 891–907, doi:10.1111/j.1365-246X.2011.05281.x, 2012. 1347

Lithospheric magnetic field post-processing

V. Lesur et al.

Title Page

Abstract

Introduction

Conclusions

References

Tables

Figures

◀

▶

◀

▶

Back

Close

Full Screen / Esc

Printer-friendly Version

Interactive Discussion



Table 1. Estimated variance of χ_m^k

	$m = k$	$m = -k$	$m \neq 0$ and $m \neq k$
$k = 0$	$\frac{v^n}{M}$	–	$\frac{v^n}{2M}$
$k \neq 0$	$\frac{3v^n}{8M}$	$\frac{v^n}{8M}$	$\frac{v^n}{4M}$

Lithospheric magnetic field post-processing

V. Lesur et al.

Title Page

Abstract

Introduction

Conclusions

References

Tables

Figures

◀

▶

◀

▶

Back

Close

Full Screen / Esc

Printer-friendly Version

Interactive Discussion

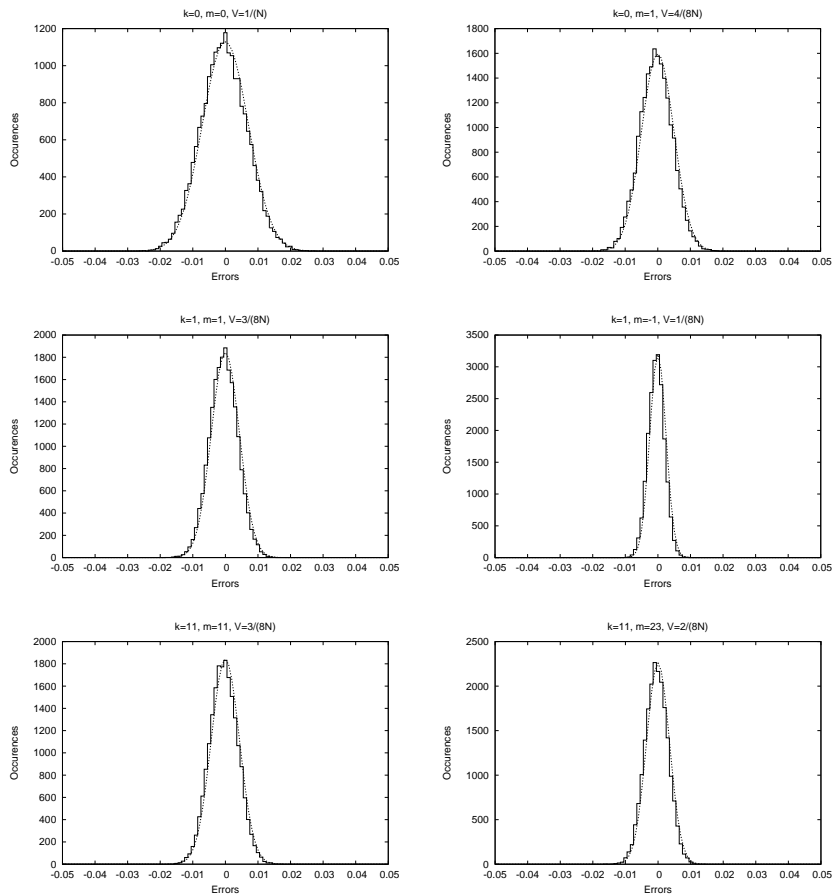


Fig. 1. Histograms of the random variable χ_m^k for several values of k and m . Is also plotted the dashed curve $\frac{M \cdot S}{\sqrt{2\pi v \chi}} \exp\{-e^2/(2v\chi)\}$ where S is the histogram step length and e the error.

Lithospheric magnetic field post-processing

V. Lesur et al.

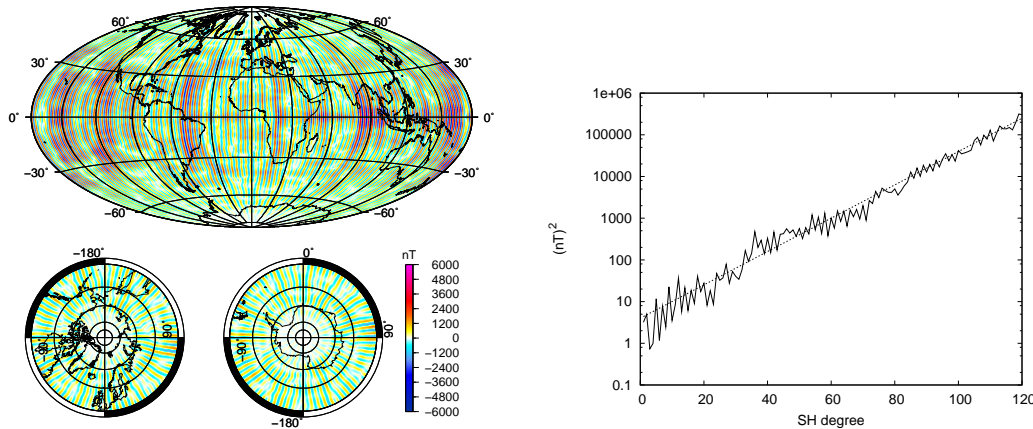


Fig. 2. Left: mapping at $r' = 6371.2$ km of the model defined in Eq. (13) where $l_1^1 = 1$, $r = 6671.2$ km – i.e. 300 km altitude, and the random variables χ_m^1 have a variance defined in table 1 using $v^l = M$. Right: associated power spectrum. The dashed line is proportional to $(\frac{r}{r'})^{2l}$.

Title Page

Abstract

Introduction

Conclusions

References

Tables

Figures

◀

▶

◀

▶

Back

Close

Full Screen / Esc

Printer-friendly Version

Interactive Discussion



Lithospheric magnetic field post-processing

V. Lesur et al.

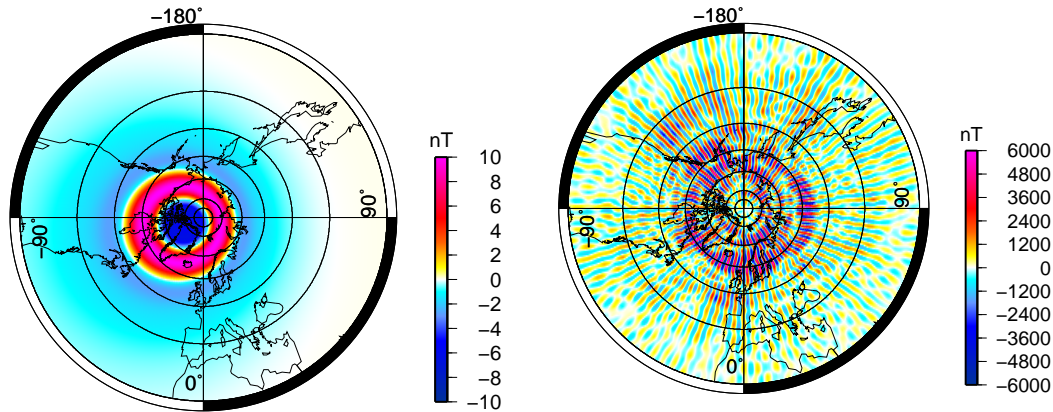


Fig. 3. Mapping at $r' = 6371.2$ km of the field of internal origin (left) and the resulting noise model (right). The data acquisition radius has been set to $r = 6671.2$ km – i.e. 300 km altitude, and the random variables χ_m^k have the variances defined in Table 1 with the ratio $\frac{v^k}{M}$ set to 1.

Title Page

Abstract

Introduction

Conclusions

References

Tables

Figures

◀

▶

◀

▶

Back

Close

Full Screen / Esc

Printer-friendly Version

Interactive Discussion



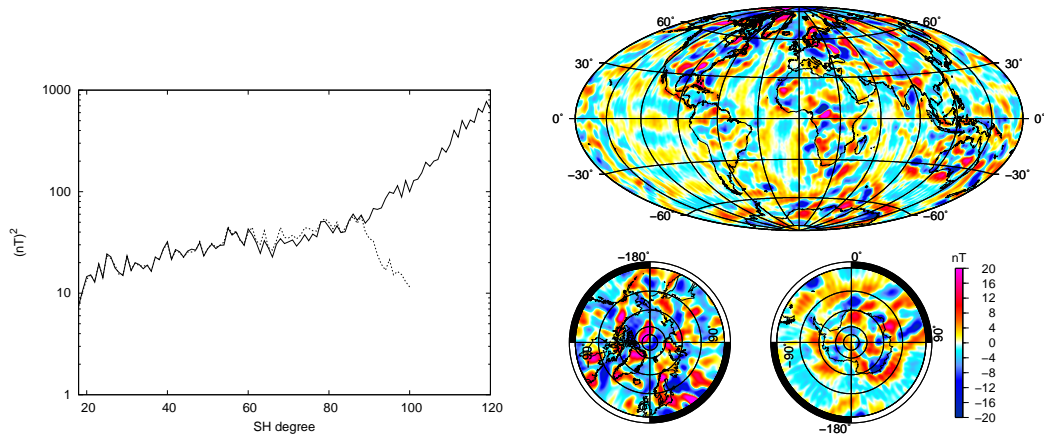


Fig. 4. Left: power spectra of the lithospheric field model (solid line) and of CHAOS-4b model (dashed line) calculated at the Earth’s surface (i.e. $r = 6371.2$ km). Right: mapping of the vertical down component of the (noisy) lithospheric field \hat{B}_i at $r = 6671.2$ km. The largest magnetic anomalies dominate, but the “along track” noise is nonetheless visible over oceanic areas.

Lithospheric magnetic field post-processing

V. Lesur et al.

Title Page

Abstract

Introduction

Conclusions

References

Tables

Figures

◀

▶

◀

▶

Back

Close

Full Screen / Esc

Printer-friendly Version

Interactive Discussion



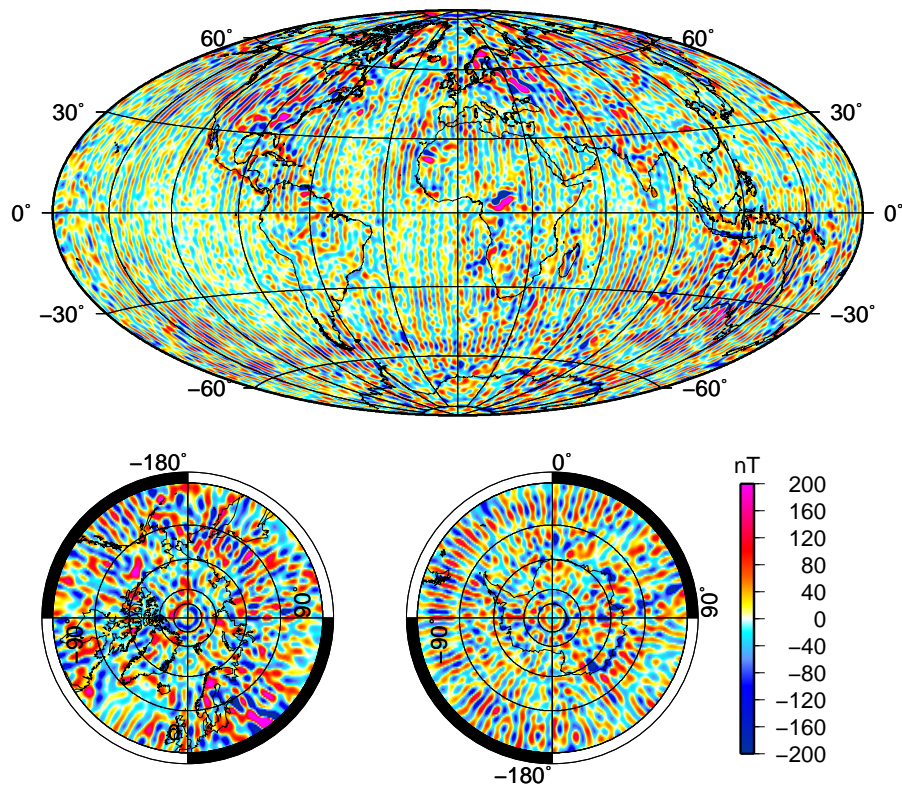


Fig. 5. Map of the vertical down component of the lithosphere magnetic field model at $r = 6371.2$ km radius derived after the step-1 of the processing chain. This corresponds to a smoothed model without co-estimation of the noise model. It is given here as a reference to be compared with Fig. 8. Along track noise is particularly visible around Antarctica, and in the Indian, Atlantic and eastern Pacific oceans.

Lithospheric magnetic field post-processing

V. Lesur et al.

Title Page

Abstract Introduction

Conclusions References

Tables Figures

◀ ▶

◀ ▶

Back Close

Full Screen / Esc

Printer-friendly Version

Interactive Discussion



Lithospheric magnetic field post-processing

V. Lesur et al.

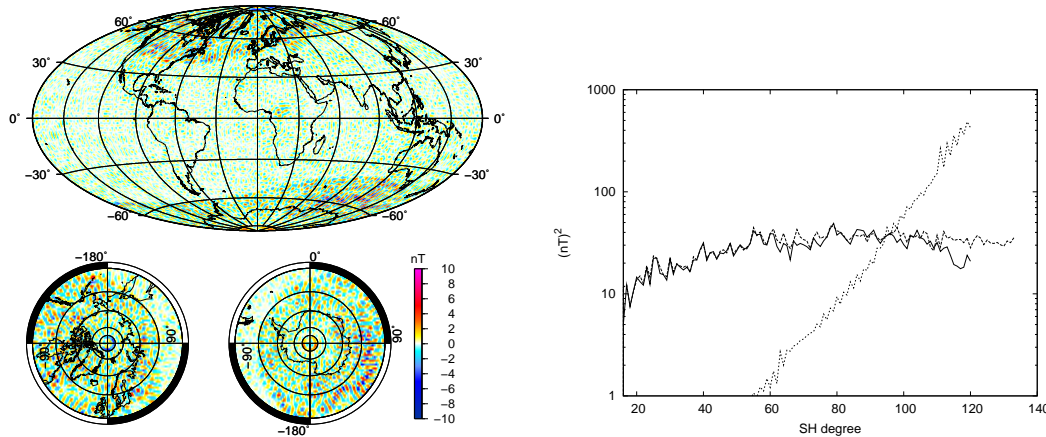


Fig. 6. Left: residuals map to the final model fit to (noisy) lithospheric field \hat{B}_l at $r = 6671.2$ km. The residuals have been scaled by a factor 10. At mid-latitudes the largest residuals are associated with the strong magnetic anomalies. The along track noise has been fitted by the noise model. Right: power spectra of the lithospheric field model B_l (solid line), of MF7 (dashed line), and the noise model (dotted line) calculated at the Earth's surface (i.e. $r = 6371.2$ km radius).

Title Page

Abstract

Introduction

Conclusions

References

Tables

Figures



Back

Close

Full Screen / Esc

Printer-friendly Version

Interactive Discussion



**Lithospheric
magnetic field
post-processing**

V. Lesur et al.

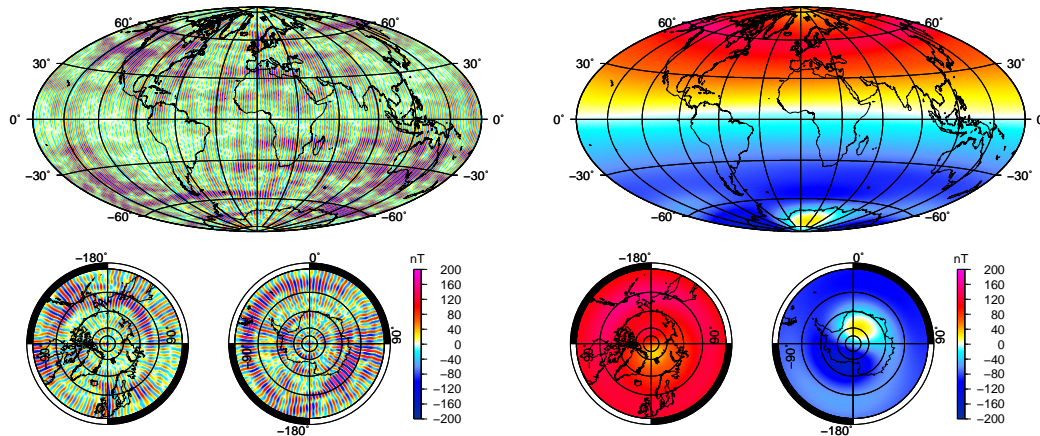


Fig. 7. Map of the vertical down components of, left, the noise model, right, the perturbation model. Both maps have been calculated at $r = 6371.2$ km radius. By definition the perturbation model is very smooth in longitude, but that does not preclude a large complexity for the noise model.

Title Page

Abstract

Introduction

Conclusions

References

Tables

Figures

◀

▶

◀

▶

Back

Close

Full Screen / Esc

Printer-friendly Version

Interactive Discussion



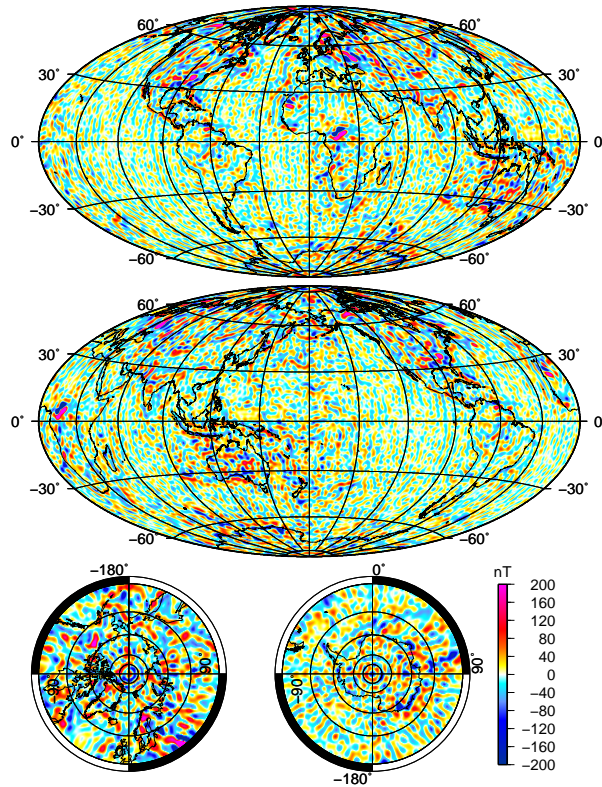


Fig. 8. Map of the vertical down components of the final lithospheric field model B_i . The map has been calculated at the Earth's surface (6371.2 km). Although some noise is still visible in the northern Atlantic and over the southern polar cap, the noise level over mid latitudes has been greatly reduced. Anomalies are particularly well defined over continents, and Indian and Pacific oceans.

Lithospheric magnetic field post-processing

V. Lesur et al.

Title Page

Abstract Introduction

Conclusions References

Tables Figures

◀ ▶

◀ ▶

Back Close

Full Screen / Esc

Printer-friendly Version

Interactive Discussion

